Investigation of Impingement of Double Orifice Synthetic Jet for Heat and Fluid Flow Characteristics in Quiescent Flow

Mukhtar Ahmad and Adnan Qayoum*

Department of Mechanical Engineering, National Institute of Technology Srinagar, Kashmir, 190006, India

ABSTRACT

Synthetic jets have been utilized for various active flow control applications including control of boundary layer transformation/detachment, lift enhancement and drag reduction, heat transfer enhancement by cooling of microprocessors in electronic industry and mixing augmentation. Numerical examination is performed to address the effects of excitation voltages and actuation frequency on the characterization of synthetic jet fluidics. The present study also explores the heat transfer improvement by a synthetic jet actuator having two cylindrical orifices arranged at the top of cavity opposite to heated thin stainless steel foil. The diameter of each orifice of the synthetic jet actuator is 2 mm with the spacing being 4 mm. The excitation voltages for actuation are taken as 20 V, 30 V, and 55 V. The computation is carried out by using Commercial software COMSOL 5.3a Multiphysics for solving three dimensional incompressible unsteady Reynolds-averaged Navier-Stokes equations with an established Shear- Stress-Transport (SST) k-ω turbulence model coupled with piezoelectric and ALE Moving Mesh technique describing the diaphragm movement. The qualities of the extracted results from the present study are authenticated by grid density, time and domain independence studies and are validated with the existing experimental data. Results show that the radial and axial velocities at the orifice exit of synthetic jet actuator tend to approach maximum at 55 V and the average heat transfer coefficient due to double cylindrical orifice is 32 % higher to that of a single orifice synthetic jet actuator with constant cavity volume thereby leading to better performance.

Keywords: Active flow control, boundary layer detachement, comsol multiphysics, heat transfer enhancement, Piezoelectric Diaphragm, synthetic jet fluidics.

INTRODUCTION

Flow control can be used to delay transition, recede turbulence, avoid separation, and to customize the flow field in many other ways. Among many active flow control devices, one of the most extensively investigated devices has been the zero-net-mass-flux actuator, which is also known as the synthetic jet actuator. Synthetic jet actuators have shown good promise in delivering flow control due to their ability to produce a continuation of vortex rings that proliferate away from an actuator orifice without any net addition of mass to the flow thus avoiding the need for any additional fluid supply.

Smith and Glezer (1998) investigated the utility of primary synthetic jet ejected from a circular orifice over a continuous jet and concluded that the prior was synthesized from the surrounding ambient fluid and consequently did not require a persistent quantity of external fluid. Mclean et al. (1999) observed high lift conventional systems by active flow control was determined as a prime contender and probably contributed 5.3% overall airplane cost, weight and drag minimization. Amitay et al. (1997) found synthetic jet actuators as an excellent alternative in modifying the various aerodynamic characteristics of bluff bodies. Crook et al. (1999) carried investigation of synthetic jet actuators for separated flow. They found that the performance of such devices depended on the geometrical parameters of the synthetic jet actuator such as orifice, cavity piezoelectric diaphragm, and electrical dynamic conditions. Holman et al. (2003) investigated the performance of an array of synthetic jet actuators for effectiveness of flow control and separation over a NACA 0025 aerofoil as a function of phase difference, excitation amplitude and the stream wise position. Rathnasingham and Breuer (2003) studied active flow control based on a real time synthetic jet over a flat plat turbulent boundary layer employing system identification method. It found that the reduction in wall pressure fluctuations by about 15% and wall shear stress by 7%. Zhou and Zhong (2009) investigated both experimental and 3-dimensional transient numerical simulations of synthetic jet actuators based on circular orifices interacting with a laminar boundary layer and observed a hierarchy of coherent structures and these reduced the wall shear stress. Chandratilleke et al. (2010) carried out numerical simulations of 2-dimensional cross-flow synthetic jet impingement in a micro channel for heat transfer improvement and observed around an increase heat dissipation up to four times. Greco et al. (2016) carried out Particle Image Velocimetry at different nozzle to plate distances (H/D). They found that for small (H/D) value the axial velocity profile of single jet showed double peak while at larger value of (H/D) it changed to bell shaped. They also found that for twin configuration the axial velocity and turbulence level increased but the impinging capacity decreased due to mixing of two jets. Jagannatha et al. (2009) performed numerical simulation of synthetic jet for fluid flow and heat transfer characteristics using shear-stress-transport (SST) k-ω turbulence model. They found that the thermal performance of the synthetic jet was highly dependent on vortex shedding, diaphragm amplitude and actuation frequency.

Gillespie et al. (2006) carried out experimental investigation of rectangular synthetic jet actuator employed particle image velocimetry (PIV) for velocity measurement. It found that substantial improvement in local convective heat transfer from a flat plate was observed due to the enhance mixing tendency of synthetic jet. Zhang and Tan (2012) experimentally performed the flow and heat transfer characteristics of the piezoelectric synthetic jet actuator with slot and circular orifices. It revealed that the synthetic jet ejected from the minor axis of the orifice spread rapidly, while the jet ejected from the major axis contracted at the beginning before spreading gradually. Im et al. (2017) utilized an efficient numerical non linear diagonal implicit harmonic balance mechanism for avoiding mesh ALE deformation of oscillating membrane and compared with the existing experimental data. It was observed that synthetic jet actuator had better stability and efficiency of fluidic characteristics. Dauphinee (1957) investigated experimentally unsteady fluid flow of synthetic jet actuator driven by mechanical or acoustics pressure waves. It was found that the standing waves were generated at the exit of orifice with constant amplitude. Cater and Soria (2002) studied flow visualization of synthetic jet actuator based on piston cylinder type actuator, using water as the operating fluid. Different categories of flow arrangement based on Reynolds number (Re) and Strouhal number (Sr) were observed. The investigation gave an indication that the synthetic jet was formed when vorticity was advected off from an actuator at a rate quicker than the vorticity diffused by viscosity. Utturkar et al. (2003) studied criteria of jet formation for comparatively thick orifice plates based on Stokes (S) numbers and Reynolds numbers (Re). It was observed that for a two-dimensional synthetic jet the value of $Re/S^2 > 2$, and for an axisymmetric synthetic jet the value of $Re/S^2 > 0.16$ at constant cavity volume. Holman et al. (2005) provided criteria of jet formation for different values of Strouhal numbers. They found that at the downstream of two orifice diameters a jet centerline velocity of 14 m/s indicates the jet formation of significant quality and strength. Agarwal and Verma (2008) proposed a similarity analysis of synthetic jet actuator in quiescent flow in the near and far field region. An identical stream wise velocity and spread rate with continuous conventional jets was predicted. Silva-Llanca et al. (2015) studied the impinging synthetic jets of high aspect ratio based on slot orifice on a stainless steel heated surface for different values of operating frequency, slot widths and distance from orifice. Peak value of Nusselt number was attained at a distance 5 slot widths from the nearest distance of the orifice exit. Qayoum et al. (2010a) studied synthetic jet actuator interacted with cross-flow over a heated flat plate laminar boundary layer. It was observed that the increase in average heat transfer coefficient was about 44% with an increase in actuation amplitude of the of piezoelectric diaphragm. Batikh et al. (2008) carried out experimental and numerical investigation for micro synthetic jet for flow control. The performance of synthetic jet actuator was modified by the augmentation of actuator frequency or by optimizing geometry of actuator and orifice. Greco et al. (2018)

performed experimental investigation of impingement synthetic jet actuator by varying the stroke length and orifice-to-plate distance. They found that at higher value of dimensional stroke length (*Lo/D*) the behaviour of heat transfer coefficient resembled that of continuous impinging jet. Paolillo et al. (2017) performed experimental investigation of quadruple synthetic jet in quiescent flow for four different configurations of varying phase lags. It was seen that behavior of synthetic jet actuator and its vortex morphology was affected leading to Structural difference in the centerline velocity distributions. Bayomy and Saghir (2017) studied the heat transfer characteristics of three different types of foam made of aluminium heat sink for electronic cooling using experimental and finite element methods. They found that for all three models there was gradual increase in local surface temperature and flow direction with increase in heat flux, decreasing the Reynolds number. Deepak et al. (2017) studied the influence of different orifice shapes on abrasive water jet by using standard k–ε turbulence model. They found that at lower nozzle radius the jet velocity and force increased. While the pressure drop at the exit of nozzle reduced exponentially. Giachetti et al. (2018) investigated synthetic jet in cross flow at various operating frequencies. With 10% increase in actuation frequency of the oscillating diaphragm, the flow behaviour favoured more turbulence and the Nusselt numbers rose to 6.5. Alimohammadi et al. (2016) utilized PIV and CFD model of adjacent synthetic in quiescent flow. It was revealed that the adjacent synthetic jet had experience same vectoring appearance under different actuation conditions. The formation and evolution of the jet solely depended on Stroke length (Lo) and Reynolds number (Re). They also found that the resultant pressure drop for both jets caused vectoring of the merged jets.

Lot of research has been carried in the direction of the characterization of synthetic jet and jet impingement from a single cavity. The influence of double orifice synthetic jet for impingement studied using piezoelectric actuator has been insufficiently examined in the literature, and such an investigation is needed.

The present study explores fluid flow characteristics along with heat transfer enhancement of double orifice synthetic jet actuator impinging on square stainless steel foil (side equal to 50 mm). Numerical simulations have been carried for studying the effect of actuation frequency and excitation voltage. The actuator diaphragm consists of a piezoelectric patch (PZT-5A) bonded on a thin copper sheet. The input material properties of diaphragm as depicted in Table 1.The synthetic jet actuator (Figure 1(a-b)) is composed of single and double orifice synthetic jets having cylindrical cavity of height, h_c= 5 mm. The diameter of vibrating diaphragm (d_c) and orifice diameter (D) are 30 mm and 2 mm respectively and the spacing between the two orifices, s =4 cm. The input heat flux (q") equal to 4000 W/m^2 is given to the stainless steel foil. The distance between the orifice plane and the heated stainless foil is equal to 120 mm. The dimension of synthetic jet actuator selection is based on Knudsen number K_n, for ensuring the continuum nature of

the fluid flow. All the dimensions of the geometry are in mm. The present computational study includes all orifice configurations (Case 1-2) as depicted in Table 2.
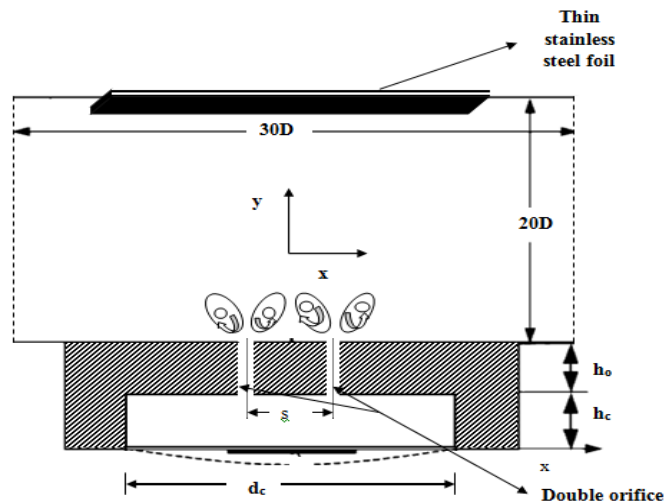
Table 1

Input properties of diaphragm

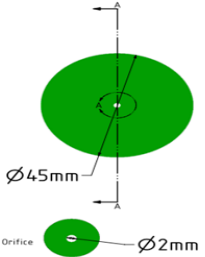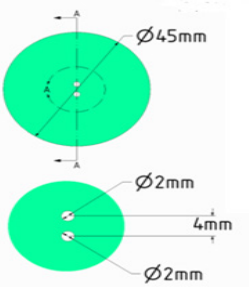| Density (P_c)	8960 kg/ m^3
Young's modulus (E)	110×10^9 N/m^2
Poisson's ratio (nu)	0.35
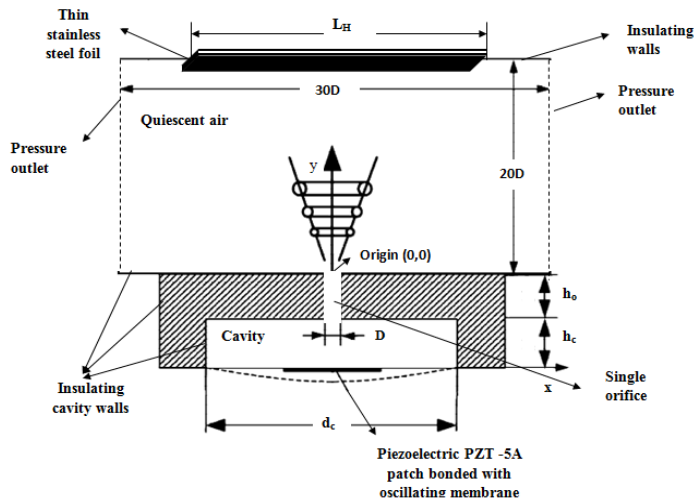
Figure 1(a-b). Geometry of the computational domain of impinging synthetic jet actuator showing different boundary conditions for single and double orifice

Table 2

Construction details of different orifice configurations for current study

Test Cases	Orifice Configuration	Dimensions of orifice
Case 1		Single Cylindrical Orifice D = 2 mm h_o = 2 mm
Case 2		Double Cylindrical Orifice D= 2 mm h_o = 2 mm s= 4 mm

DETAILS OF COMPUTATIONAL STUDY

This section presents the fluid flow and heat transfer characteristics of low-Reynolds number turbulent impinging synthetic jet actuator in a quiescent surroundings. The most difficult part in the simulation of synthetic jet actuator is the handling of the vibrating diaphragm. Details of numerical simulation such as computational geometry, mesh, boundary conditions, grid generations study along with solver control, convergence criteria and quiescent domain independence study results are also presented. The present computation study uses COMSOL 5.3a Multiphysics for three dimensional incompressible unsteady Reynolds-averaged Navier-Stokes (RANS) equations with an established Shear-Stress-Transport (SST) k-ω turbulence model coupled with the user defined ALE Moving Mesh technique describing the diaphragm movement to ensure correct depiction of the near-wall region of wall-bounded turbulent flows. The outlets boundaries are specified with turbulent intensity of 4 percent and the value of wall function to displace the nearest wall mesh y^+ is equal to 1. Finite element method is employed for solving the governing equations of heat transfer, fluid flow and piezoelectricity. The computational domain of synthetic jet actuator comprises of three zones in conjunction with the cavity, the orifice, and the surrounding quiescent region into which the jet interacts. Since actuation is done to

piezoelectric patch (PZT-5A), piezoelectric effects need to be considered. Piezoelectricity combines the electrical behavior of the material and the material stress and strain. The periodic oscillating of diaphragm performs by the action of inverse piezoelectric effect on the application of electric field **E** inducing stresses **–eE** which tends to align the internal dipoles is as given by equations as.

$$\sigma = c^E S - eE \qquad\qquad ... (1)$$
$$D = eS + \varepsilon^s E \qquad\qquad ... (2)$$

where **E** is the applied electric field, σ is the stress in the piezopatch material, **eS** is the induced polarization due to strain **S**, ε^s is the permittivity coefficient under constant strain. **D** is the dielectric displacement **e** is the coupling matrix and c^E is the stiffness coefficient under constant electric field.

The applied voltage at the bottom of piezo patch is given by

$$V = V_{exc} Sin\omega \qquad\qquad ... (3)$$

where V_{exc} is the excitation voltage amplitude, V is instantaneous voltage and ω is angular frequency of the diaphragm. When the electric potential V_{exc} is applied at the bottom of piezoelectric membrane. The piezoelectric material makes a normal force along the *y*-axis by the *y*-component of the electric field. This will cause displacement in the membrane by (e_{22}) element of coupling matrix **(e).**

The governing equations of the fluid inside the cavity, the surrounding medium and heat source is modeled by the incompressible Navier-Stokes equations and energy equations are given by

$$\rho \frac{\partial u}{\partial t} + \rho(u.\nabla)u = \nabla.\left[-pI + (\mu + \mu_T)(\nabla u + (\nabla u)^T)\right] + F \qquad\qquad ... (4)$$

$$\rho\nabla.u = 0 \qquad ... (5)$$

$$\rho C_p \frac{\partial T}{\partial t} + \rho C_p u.\nabla T + \nabla.q = Q \qquad\qquad ... (6)$$

where q= -k∇T

where μ is the dynamic viscosity, μ_T is the turbulent viscosity due to velocity fluctuations, ρ is the fluid density, **u** is the velocity field in the computational domain, **p** is fluid pressure field and **F** is a volume force field. SST k–ω turbulence model also consists of two equations, the turbulence intensity equation (k), and the rate of turbulence dissipation (w), respectively. The turbulence intensity equation is given by

$$\rho(u.\nabla)k = \nabla.\left[\left(\mu + \frac{\mu_T}{\sigma_k}\right)\nabla k\right] + p_k - \rho w \qquad\qquad ... (7)$$

The rate of turbulence dissipation equation is given by

$$\rho(\mathbf{u}.\nabla)w = \nabla.\left[\left(\mu + \frac{\mu_T}{\sigma_g}\right)\nabla w\right] + \alpha\frac{w}{k}p_k - \beta\rho w^2/k \qquad \text{…(8)}$$

The material properties of working fluid and input parameters for piezoelectric membrane in the governing equations are

ρ =1.225 kg/m^2, Cp = 1.00 kJ/kg.K, k = 0.0254 W/m-K, V_{exc} = 20- 55 volts, α=1.44 , ß = 1.92 and σ_k= 1.0

According to (Holman et al., 2005) a synthetic jet is formed when a non-dimensional number criterion is satisfied. The criterion states that when the inverse of the Strouhal number is larger than a constant a jet is formed

$$\frac{1}{S_r} > C \qquad \text{… (9)}$$

where C is constant depends on the geometry of synthetic jet actuator and is equal to 1. Strouhal Number, S_r is defined as

$$S_r = \frac{Re}{S_t^2} \qquad \text{... (10)}$$

The Reynolds number is defined in equation as

$$Re = \frac{U_o D}{\nu} \qquad \text{… (11)}$$

The characteristics velocity of synthetic jet is given by

$$U_o = L_o f = \frac{1}{T}\int_0^{T/2} \mathbf{u}_t \, dt \qquad \text{… (12)}$$

Where U_o is the characteristics (average) velocity of synthetic jet at the exit of orifice during the half of expulsion stroke, f is the actuation frequency of the synthetic jet actuator, L_o is the stroke length (defined as the length of slug travels during the ejection portion of the oscillation), T/2 is the half period of diaphragm oscillation and $\mathbf{u}_t$ is the instant velocity at the orifice discharge plane.

The Stokes number based on actuation frequency and orifice diameter of synthetic jet actuator is given by

$$S_t = \sqrt{\frac{2\pi f D^2}{\nu}} \qquad \text{… (13)}$$

For heat transfer investigation, the heat flux is given to the heated surface (q"). The average convective heat transfer coefficient (h_{avg}) is given by

$$h_{avg} = \frac{q''}{T_s - T_a} \qquad \text{…(14)}$$

where T_s the average temperature on the heated surface and and T_a is the bulk ambient temperature of fluid. The local mean bulk fluid temperature is a weighted average temperature of fluid and is evaluated at every point in stream-wise direction.

GEOMENTRY AND MESH

The synthetic jet actuator consists of two domains, the first composed of bottom piezoelectric membrane wall, cavity and orifice, and the second consists of the ambient surrounding fluid. No slip boundary condition is applied at the side and top walls of cavity. The oscillating piezoelectric diaphragm and cavity surfaces are treated as nonporous. The left and right wall of outer domain comprising of ambient fluid (in which the jet is expelled) is specified with pressure outlet conditions. For heat transfer analysis adiabatic conditions were applied at the cavity walls and lower and upper walls of outer domain. The thin stainless steel is maintained at constant heat source of 4000 W/m^2. The geometry of synthetic jet actuator along with heated stainless steel foil shown in Figure 1 has been meshed with structured mesh grid (triangular elements) for cavity and orifice exit. The unstructured free triangular scheme is selected to concede for the relative prescribed displacement among the nodes on the diaphragm for successful coupling with the fluid flow. The outer fluid domain and heated surface are meshed with quadrilaterals structured scheme. Adiabatic boundary conditions were activated at the outer fluid domain walls, cavity walls and the piezoelectric oscillating diaphragm. The fluid inside the orifice, the cavity and in the surrounding medium treated as is incompressible. The ambient temperature of 300 K under standard air conditions is also specified. A sample mesh of synthetic jet actuator fluidics combines with heat transfer due to stainless steel foil domain demonstrating each substitute point is exhibited in Figure 2.
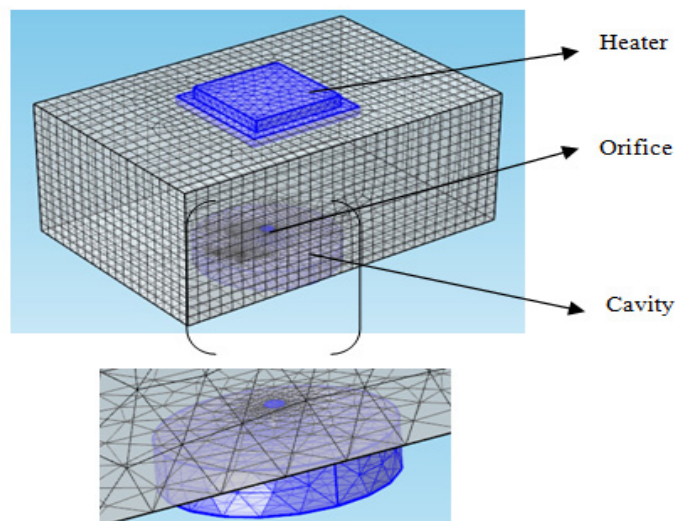

Figure 2. Computational grid for solution domain in present investigation [inset shows extended outlook of the marked region] at operating frequency 15Hz and excitation voltage is 20 volts

INITIAL CONDITIONS AND SOLUTION METHODOLOGY

The initial location of the piezoelectric diaphragm is at rest. Special moving mesh ALE techniques is formulated and combine with the piezoelectric and conjugate heat transfer module of Comsol 5.3a Multiphysics solver to describe the periodic motion of the piezoelectric diaphragm subjected to a sinusoidal electric field. A time dependent implicit solver formulation has been carried out for the numerical algorithm.

GRID INDEPENDENCE STUDY

Similar to the approach adopted by (Jain et al., 2011) and (Yue-Wei et al., 2014) simulation results in the present investigation were resolved following a precise time and grid independence study. The mesh density appeared to have a greater impact on the instantaneous exit velocity of synthetic jet actuator. The relative error in the maximum velocity at the orifice exit for the medium grid mesh consisting of 290000 elements and the coarse grid mesh of 230000 elements with respect to the fine mesh of 380000 elements was 4% and 12.7% respectively. Based on the actuation frequency (f) a time step of $1/2000f$ is chosen to allow for 2000 time steps per cycle for computing both ejection and suction portion of synthetic jet actuator as shown in Figure 3 and 4 respectively.

For maintaining balance between computational time economy and efficiency, a medium mesh grid consisting of 290000 elements had been chosen for final computation. In case of domain independent investigation for the near field of the jet, the size of outer domain was chosen as 20 orifice diameter (along the axis) and 30 orifice diameters (sideways) was sufficient for visualization of clockwise vortices.
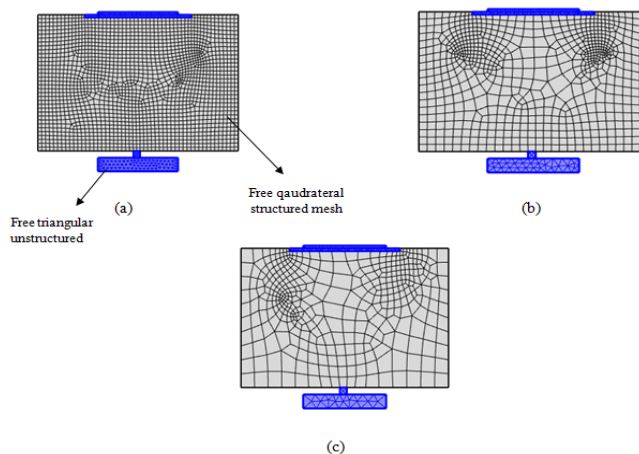

Figure 3. Overall view of the free triangular and free quadrateral mesh schemes of synthetic jet actuator at different mesh densities; (a) fine mesh (b) Medium (c) coarse mesh at operating frequency 15 Hz and excitation voltage 20 volts
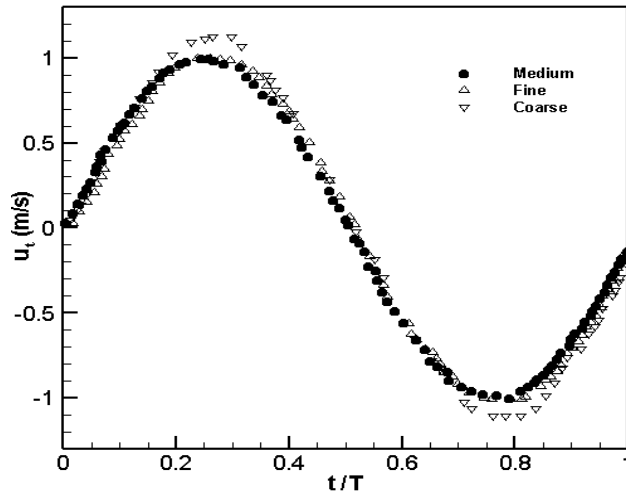
Figure 4. Instantaneous jet velocity (u_t) variation of a synthetic jet actuator for three different mesh density at axial distance (y/D =0) operating at frequency, *f*=15 Hz and excitation voltage 20 volts

SOLVER CONTROL AND CONVERGENCE

The excitation was applied to the piezoelectric diaphragm and the flow in the outer domain was initialized at rest. Each unsteady simulation was run for about five to six cycles until the converged solution was obtained. The employed convergence criterion required that the scaled residuals decrease to 10^6 for all the governing equations. On the attainment of the value of 10^6 the jet exit velocity showed no noticeable variation and present simulation was considered to be converged.

VALIDATION WITH THE EXPERIMENT

Before initiating the computations for synthetic jet actuator, the zero net mass flux over a cycle of synthetic jet actuator could be confirmed by velocity time fragments at various radial positions close to the orifice exit as shown in Figure 5. For an excitation voltage amplitude of 30 volts and an actuation frequency was set to equal 951 Hz. The peak value of velocity during suction was lower in comparison to blowing phase. The percentage deviation between the present and the results revealed by Qayoum et al. (2010b) is 12.8%. The possible reason for the deviation may be due to the hotwire incapability of track down the flow direction.

   Figure 5, Figure 6, Figure 7 and Figure 8 compare the instantaneous, radial, 2-D velocity contours and axial profile of synthetic jet actuator in blowing phase at the centerline of the orifice (x/D=0) and (z/D=0) with the experimental results of Qayoum et al. (2010b) under identical conditions. The jet axial velocity first increased to a maximum value with
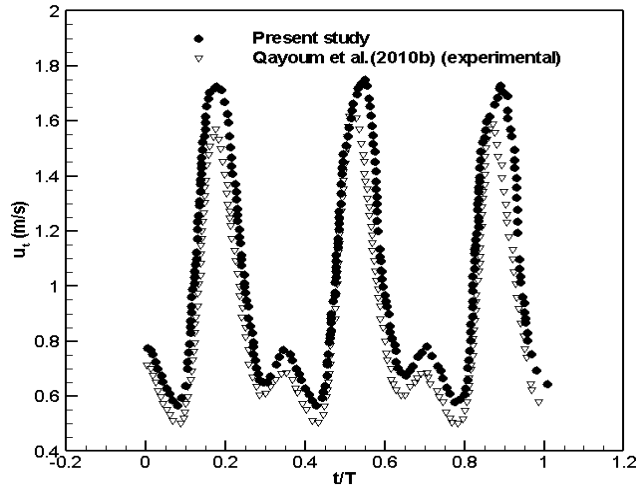
Figure 5. Comparison of time fragments of instantaneous jet velocity (u) at radial positions (x/D=0) corresponding to the axial position (y/D) = 0.5 with (Qayoum et al., 2010b). The excitation voltage amplitude is prescribed to 30 V at excitation frequency of 951 Hz. The diameter of orifice, D= 0.5mm
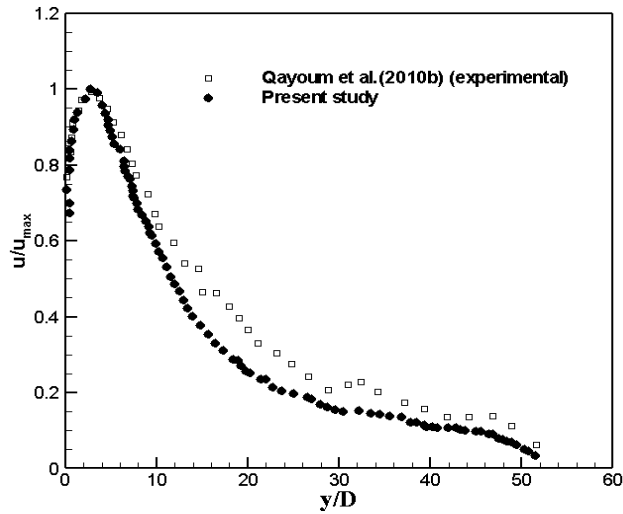

Figure 6. Comparison of jet centerline velocity (u_{cl}/u_{max}) in the axial direction (y/D) with (Qayoum et al.,2010b). The excitation voltage amplitude is chosen as 30 V at an actuation frequency of 951 Hz. The diameter of orifice, D= 0.5mm
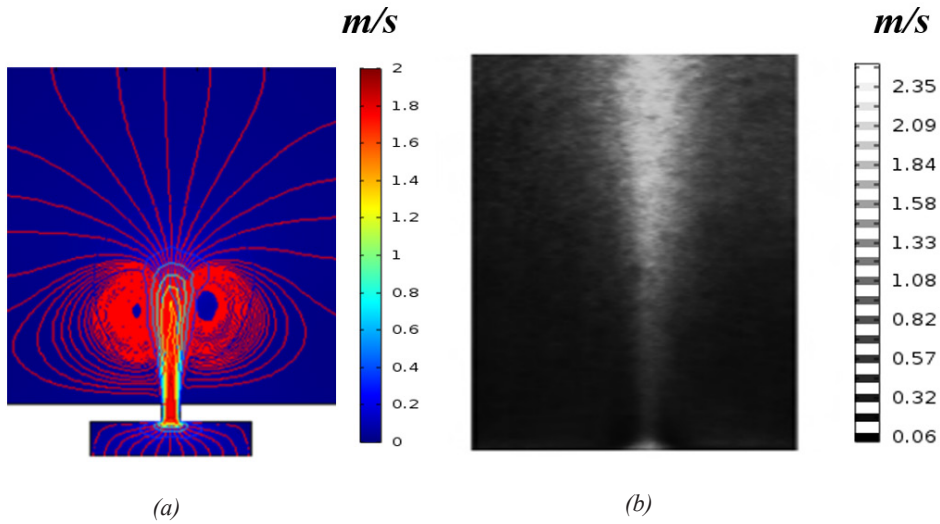
(a) *(b)*

Figure 7. Comparison of 2-D instantaneous velocity body contour: (a) present computational model (b) Schlieren images from (Qayoum et al.,2010b) for single jet at an excitation voltage of 55 volts and Orifice diameter, D= 2 mm. The carrier frequency is equal to 475 Hz.
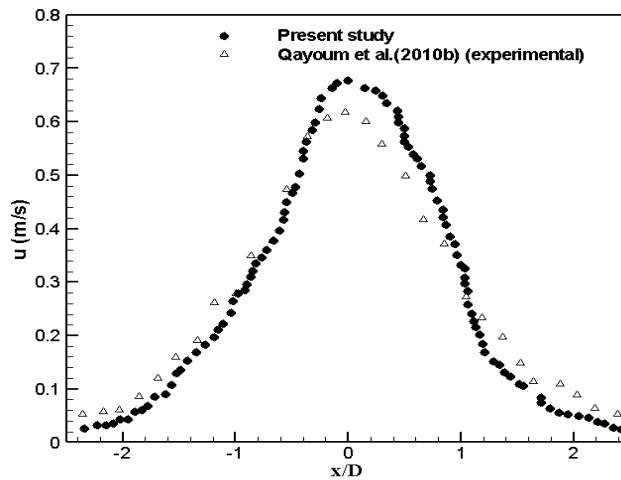

Figure 8. Comparison of radial velocity profiles of synthetic jet actuator with (Qayoum et al., 2010b) at axial position, y/D= 6 operating at frequency, f=951 Hz and excitation voltage, V_{exc}= 30 volts

successive reduction to zero velocity in the surrounding quiescent air. In Figure 7 the percentage deviation between the present and existing experimental results was 13.3%. The velocity profiles in Figure 5, 6, 7 and 8 follow the same trend and matches in a reasonable manner with the experimental results of Qayoum et al. (2010b).

RESULTS AND DISCUSSIONS

Synthetic jets are characterized by the evolution, advection and dispersion of vortex rings. The present study reports the influence of synthetic jet promulgate from a double orifice and impinging on a stainless steel heated plate placed in quiescent air. The intensity of the interaction of the synthetic jet actuator with the surrounding quiescent flow relies upon the strength of the vortices generated at the orifice exit and their momentum transported over the surface. The synthetic jet actuator parameters are a function of surface heat transfer coefficient distribution giving data on the effectiveness of the jet for heat transfer enhancement. The reason for an increase in heat transfer is on account of temporal and spatial flow patterns. This is exhibited by the velocity (in axial and radial directions) and temperature profiles. Numerical results are presented in the terms of velocity and temperature profiles.

Velocity Profiles

Figure 8 shows surface velocity contour of a single orifice synthetic jet actuator at different times namely, T/8, T/4, 3T/8, T/2, 5T/8, 3T/4, 7T/8 and T in quiescent conditions operated at excitation voltage of 55 V and frequency of 15 Hz. Different shapes of the velocity contours versus-time were generated in one cycle from the simulation.

The exit velocity of synthetic jet actuator was maximum at the centre of orifice. As we went away from orifice velocity decreased exponentially and becomes zero at the far away field due mixing of synthetic jet with the external quiescent flow field. The vortex rings appearing at the centre of orifice again justified maximum velocity at the centre.

At the start of the expulsion cycle (shown in T/8), the fluid near the side of the orifice moved out first increasing the velocity (Figure 9(a)-9(c)). When the diaphragm moves further out, more fluid was expelled, but the fluid coming from inside the cavity encounters the resistance from the fluid moving in the opposite direction which resulted in the drop in the velocity momentarily as in figure 9(d).

Figure 9(b) depicts the simulation results corresponding to time T/4. As the diaphragm oscillated, the ambient air was alternately drawn into and expelled out from the cavity orifice. The upward movement of the diaphragm led to the formation of shear layer at the edge of orifice. A vortex ring was formed by the roll up of ambient air induced by the vorticity. Figure 9(c) and 9(d) correspond to times T/2 and 3T/8 during which the diaphragm is still moving upwards. The fluid continuously came out from the opening and a vortex pair was formed as in Figure 9(c). There was a drop in velocity seen in Figure 9(d) due crossing over of the vortex pair.

Figure 9(e-h) corresponds to times 5T/8 to T during which the diaphragm moves downwards to entrain the fluid into the cavity. After the vortex crossover there was a decrease in velocity. During the suction period the air was sucked near the walls. There was lowering of suction pressure and flow was sucked in from a wider area in front of orifice. The vortex pair moved towards the diaphragm.
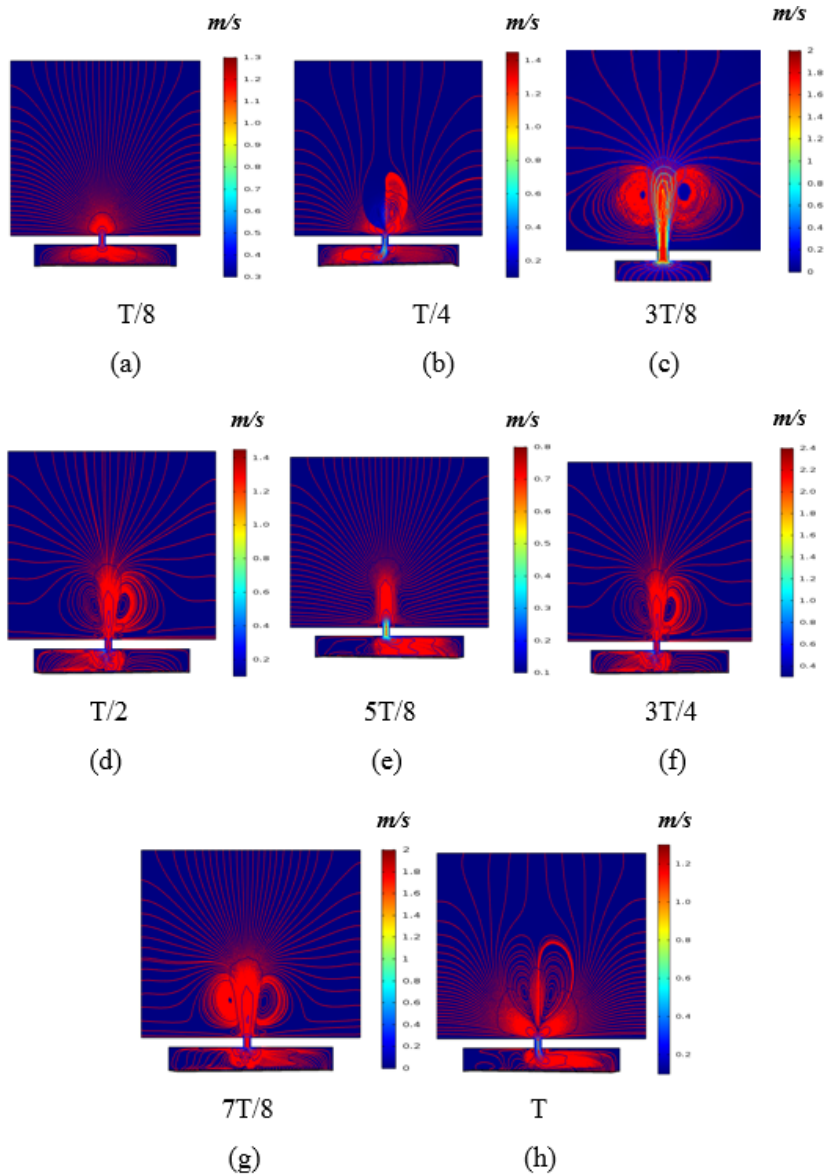

Figure 9. Velocity contours for different times in a cycle of operation for single orifice synthetic jet actuator at *f*= 15 Hz , Re =330 and V_{exc} =55 volts

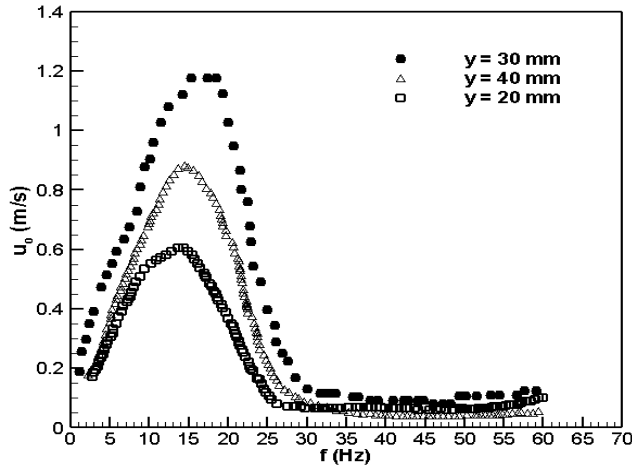*Figure 10.* Mean centerline velocity of single orifice synthetic jet actuator at radial location (x/D =0) under different actuation frequencies at excitation voltage of 55 volts

Figure 10 shows mean centerline velocity of single orifice synthetic jet actuator at an excitation voltage of 55 V for different actuation frequencies at different axial distances. It is seen from Figure 10 that at 15 Hz frequency mean centre line velocity is maximum at all axial distances. The mean velocity increased with the increase in the axial distance. At the axial distance (y=15 mm) the mean velocity was maximum.
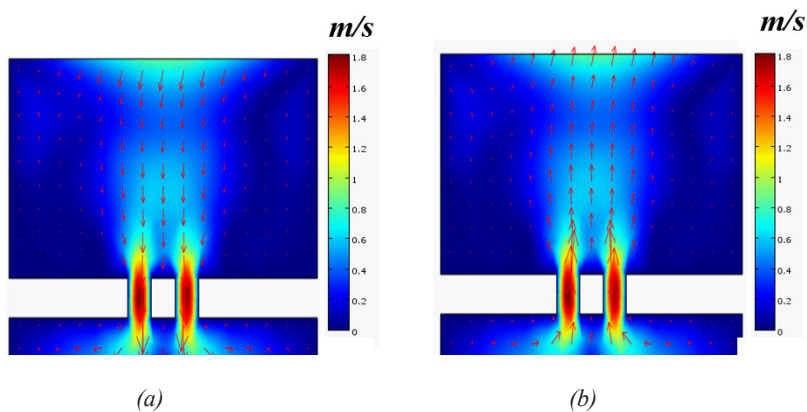

(a)   *(b)*

Figure 11. Surface velocity profile of double orifice synthetic jet showing: (a) suction (b) ejection operating at frequency of 15 Hz, Re = 247 and V_{exc} = 55 volts at time, t = 3T/8

Figure 11 shows velocity vector profile of the double orifice synthetic jet showing suction and ejection. It is quite evident from Figure 11 that near the wall the velocity was maximum as the two synthetic jets combined to form the central jet which built a greater fluid momentum and efficient mixing.

Figure 12. Velocity contours for different times in a cycle of operation for double orifice synthetic jet actuator at f= 15 Hz and V_{exc} =55 Hz

Figure 12 shows surface velocity profile of the double orifice synthetic jet showing suction and ejection at different times namely, T/8, T/4, 3T/8, T/2, 5T/8, 3T/4, 7T/8 and T in quiescent conditions operated at excitation voltage of 55 V and frequency of 15 Hz. It is quite evident from ‑ Figure 12 that near the wall the velocity was maximum as the two synthetic jet combine to form the central 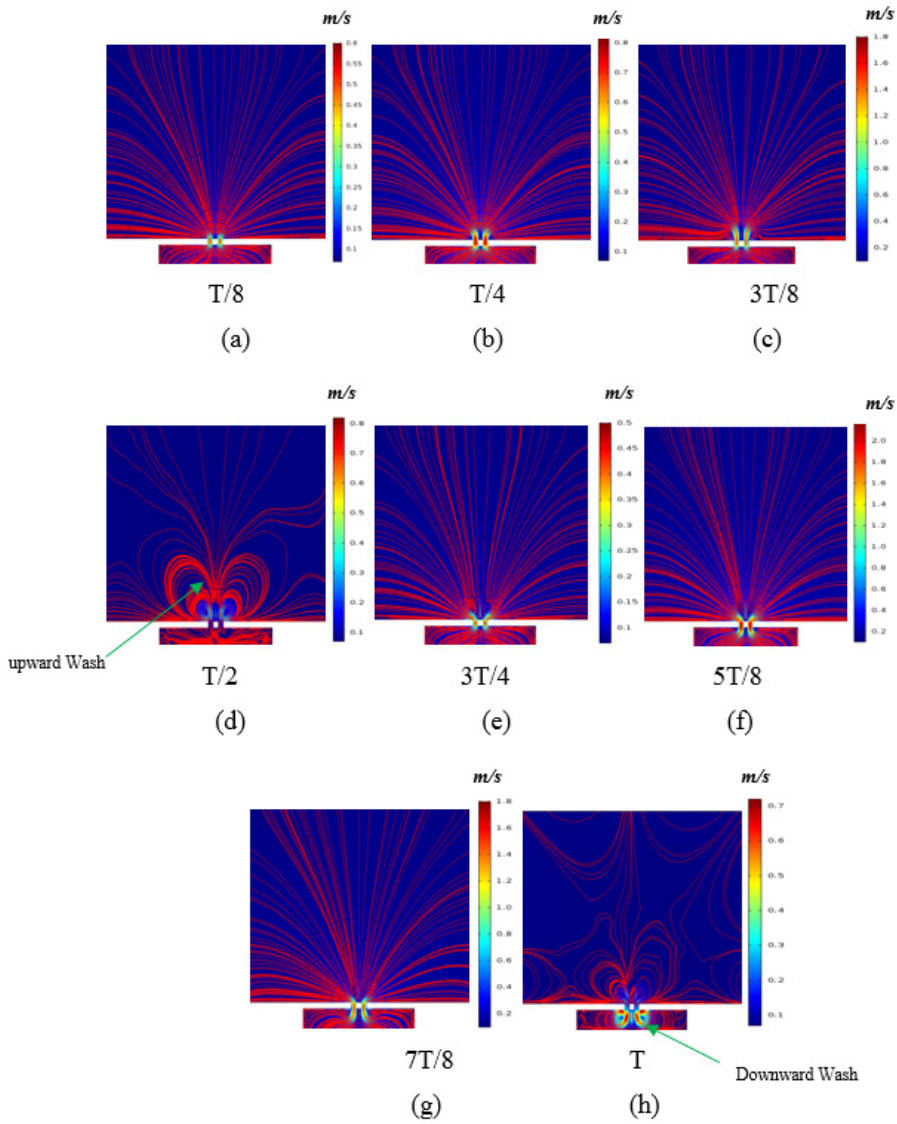jet which built greater fluid momentum and efficient mixing. Figure 12 shows a lower velocity for the double-orifice jet configuration

as compared to single orifice jet similar to the results observed by Qayoum et al. (2010b). The reason for the lower velocity may be due to greater mixing of the vortices generated in case of double-orifice. At the start of the expulsion cycle (shown in T/8), the fluid near the side of the orifices moves out first increasing the velocity (Figure 12(a)). Figure 12 (b-d) depicts the simulation results corresponding to time T/4 to T/2 during which the diaphragm is still moving upwards. The fluid continuously came out from the opening and a vortex pair was formed upward wash as in Figure 12(d). There was a drop in velocity seen in Figure 12(e) due crossing over of the vortex pair. Figure 12(e-h) correspond to times 5T/8 to T during which the diaphragm moved downwards to entrain the fluid into the cavity. During the suction period the air was sucked near the walls. There was a lowering of suction pressure and flow was sucked in from a wider area in front of orifice. The vortex pair moved towards the diaphragm forms downward wash as seen in Figure 12(h).

Figure 13 and Figure 14 present the axial and radial velocity development of the synthetic jet at the various excitation conditions at time 2T/8. The excitation conditions used were 20 volts, 30 volts and 55 volts at a frequency of 15 Hz. The mean velocities along the jet centerline were seen to decrease with an increase in the axial and radial distance from the orifice. As seen from the figure the centerline axial velocity increased with an increase in excitation voltage and tends to maximum at 55 volts. This is due to maximum displacement attained by piezoelectric diaphragm (by the action of inverse piezoelectricity) which is responsible for maximum ejection of fluid from inside the cavity to orifice exit. The radial velocity followed the same trend as it increased due to increase in excitation voltage and reached a maximum at 55 volts.
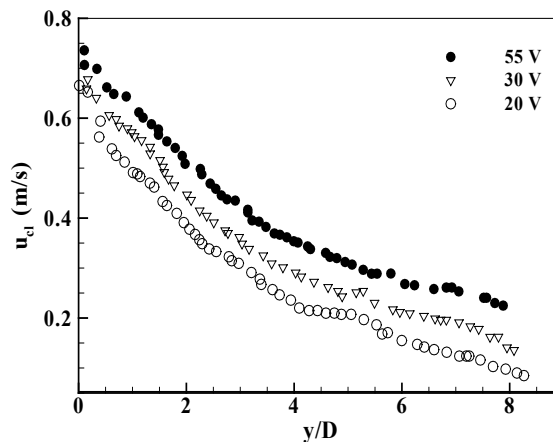

Figure 13. Effect of excitation voltage on the mean centerline velocity along axial direction (y/D) due to single orifice synthetic jet actuator at a location of x/D=0. The excitation voltage are equal to 20 volts, 30 volts and 55 volts respectively
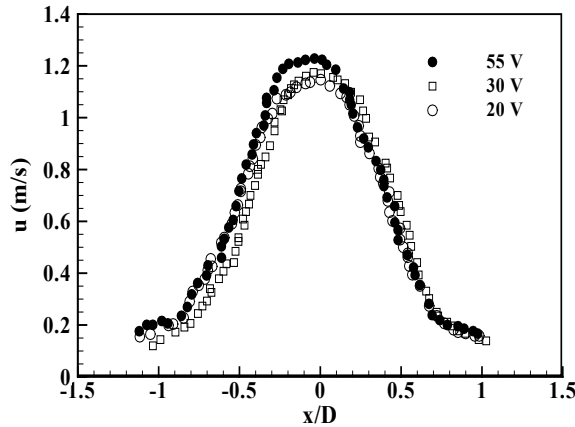
Figure 14. Effect of excitation voltage on the mean centerline velocity in radial direction (x/d$_o$) due to single orifice synthetic jet actuator at an axial location of z/d$_o$=20 The excitation voltages are equal to 20 volts, 30 volts and 55 volts respectively
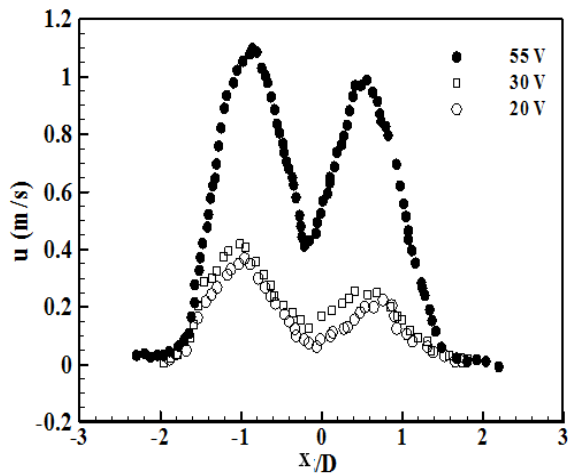

Figure 15. Mean radial velocity (**u**) in the spanwise direction (x/D) at the axial location y/D=20 for 20 volts, 30 volts and 55 volts excitation conditions with both Jet1 and Jet2 running simultaneously operating frequency set to 15 Hz

Figure 15 presents the radial velocity profiles for the double orifice synthetic jet configuration. It was observed from the figure that the highest average radial fluid velocity was attained at an excitation of 55 volts but lower as compared to single orifice synthetic jet. This is due to the fact that at far off fields individual synthetic jets merge to enhance mixing and ultimately the velocity gets reduced. This further confirms the broadening of the two-jet system.

Heat Transfer Coefficient

The distribution of surface temperature on the surface of heated stainless steel as a function of the synthetic jet actuator parameters gives information on the effectiveness of the jet for heat transfer enhancement.
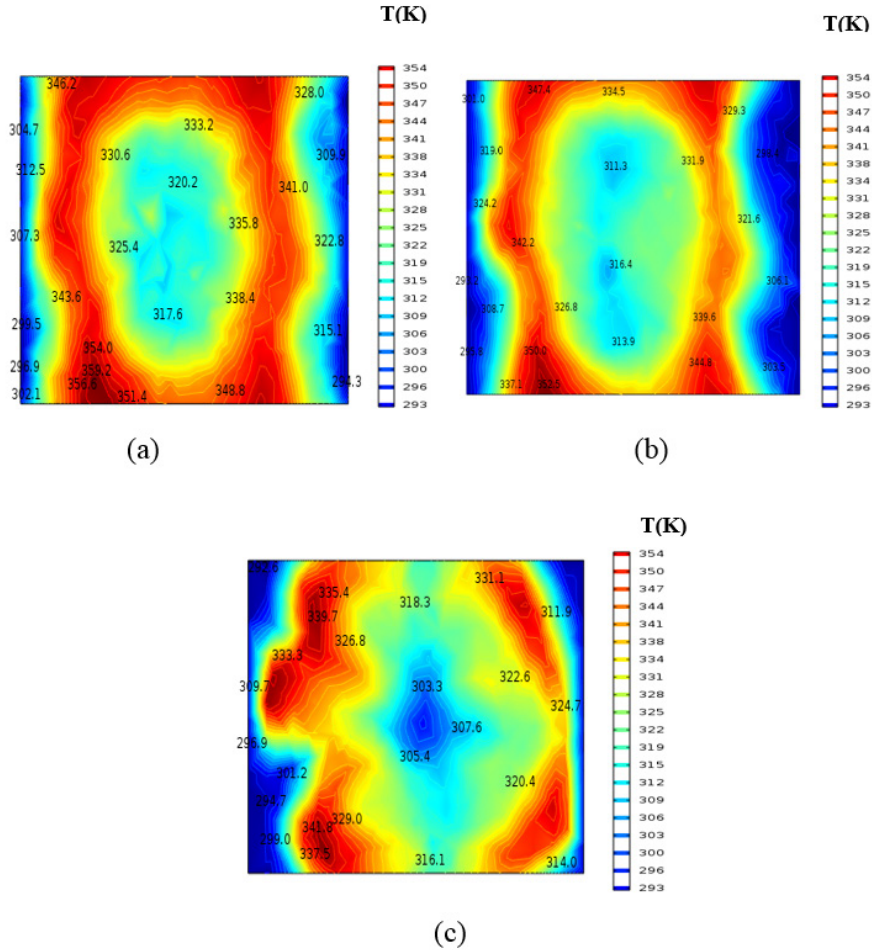

Figure 16. Temperature contour on heated plate simulated after impingement for double orifice synthetic jet actuator in quiescent flow: (a) V_{exc} = 20 volts; (b) V_{exc} = 30 volts; (c) V_{exc} = 55 volts at operating frequency, f =15 Hz and q"= 4000 W/m^2

Figure 16 shows the temperature distributions for a plate heated by the constant heat-flux (4000 W/m^2) subjected to the impingement of double orifice synthetic jet at an actuation frequency of 15 Hz for different excitation voltages. The spacing between the heated stainless foil and orifice exit plane was chosen as 120 mm. Figure 16 shows a lower temperature distribution at excitation voltage equal to 55 volts implying increased heat removal rate as compared to other excitation conditions.
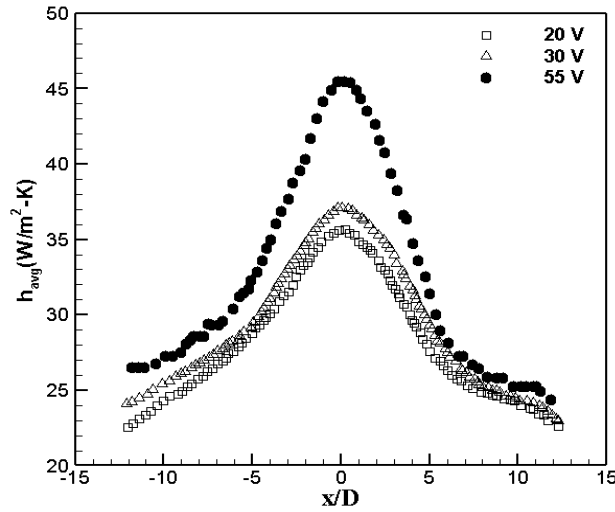
Figure 17. Heat transfer coefficient due to impingement of double orifice synthetic jet actuator actuation frequency, f=15 Hz and y = 120 at different excitation voltages

Figure 17 shows the corresponding average heat transfer coefficient for double orifice synthetic jet actuator. The maximum heat transfer coefficient equal 45 W/m^2-K was observed corresponding to 55 volts at the centre of impingement plate. This is due to greater amplitude of oscillation generated by piezoelectric membrane as the applied voltages elevates from 20 volts to 55 volts respectively.

Figure 18 shows the comparison of average heat transfer coefficient for single and double orifice synthetic jet actuator operated at an actuation frequency of 15 Hz and excitation voltage equal to 55 volts. For constant orifice diameters, it was seen that heat transfer coefficient was high in case of double orifice synthetic jet. The difference in the
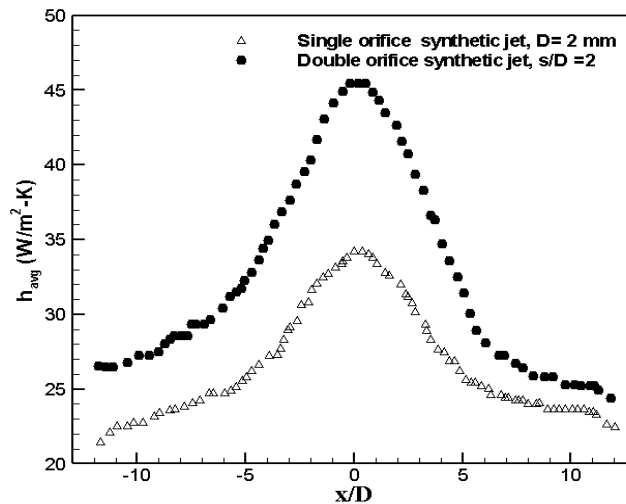

Figure 18. Comparison of heat transfer coefficient due to impingement of single and double orifice synthetic jet at y = 120 operated frequency, f=15 Hz and excitation voltage 55 volts

heat transfer coefficient actuator was approximately 32%. The high values of heat transfer coefficient for double orifice jets are attributed to large magnitude of the clockwise vortices at the orifice exit compared to single orifice jet. This results in enhanced mixing in the region between the interacting ambient fluid and near the stainless steel foil leading to increase in average heat transfer coefficient.

As seen from Figure 17 and 18, the heat transfer enhancement solely depended on the quantity of orifices employed in the synthetic jet actuator but independent upon its size operating at optimum excitation conditions.

CONCLUSIONS

The detailed computational study on the effect of excitation voltage and actuation frequency of a single cavity having double orifice synthetic jet actuator on fluid flow and heat transfer enhancement has been carried. The following important observations can be summarized as:

1. The velocity of synthetic jet with single and double circular orifice reaches a maximum value to form upward wash vortices when operated at its optimum resonant frequency.
2. The average heat transfer coefficient due to double orifice synthetic jet is 32% higher as compared to single orifice synthetic jet at optimum frequency and voltage.
3. The mean centerline and radial velocities along the synthetic jet increases gradually for an excitation voltage varies from 20 volts to 55 volts in a non-linear pattern. This is due to piezoelectric diaphragm displacement being a non linear function of applied electric field.
4. The mean radial velocity of double orifice synthetic jet is lower as compared to single orifice due to mixing enhancement and greater magnitude of clock wise vortices.
5. The interaction of double orifice synthetic jet impingement shows a general increase in heat transfer enhancement with an increase in excitation voltage. A maximum enhancement in heat transfer is equal 45 W/m^2-K is observed at 55 volts amplitude of excitation.
6. The heat transfer enhancements solely depend on the quantity of orifices employed in the synthetic jet actuator but independent upon its size operating at optimum excitation conditions.

ACKNOWLEDGEMENT

NOMENCLATURE

d_c	Cavity width	[m]
D	Orifice width	[m]
f	Diaphragm actuation frequency	[Hz]
h_c	Height of cavity	[m]
h_o	Height of orifice	[m]
h_{avg}	Average heat transfer coefficient	[W/m²-K]
L_h	Lengths of thin stainless steel foil	[m]
p	Pressure	[Pa]
q"	Heat flux	[W/m²]
Re	Reynolds number, dimensionless	
s	Spacing or pitch between two orifices	[m]
S_r	Strouhal number, dimensionless	
S_t	Stokes number, dimensionless	
T	Time period of oscillation	[sec]
T_s	Average surface temperatures of thin stainless steel foil [K]	
T	Bulk fluid temperature	[K]
u	Mean radial velocity of synthetic jet	[m/s]
u_{cl}	Mean centerline velocity of synthetic jet [m/s]	
u_t	Instantaneous velocity of synthetic jet	[m/s]
u_{max}	Maximum axial velocity of synthetic jet [m/s]	
V	Instantaneous voltage	[volts]
V_{exc}	Excitation voltage amplitude	[volts]
x	Coordinate along major axis of stainless steel foil [m]	
y	Coordinate normal to the stainless steel foil [m]	

Greek symbols

ρ	Density of air [kg/m³]	
μ	Dynamic viscosity [kg/ms]	
μ_t	Turbulent viscosity[kg/ms]	
v	Kinematic viscosity[m²/s]	
C^E	Stiffness Matrix [C/mV]	
E	Electric field [N/C]	
ε	Dielectric constant[F/m]	
σ	Stress in piezoelectric patch[N/m²]	

Subscripts

a	Ambient air	
s	Surface	
o	Average	
cl	Centreline	
t	Instantaneous	

REFERENCES

Agarwal, A., & Varma, G. (2008). Similarity analysis of planar and axisymmetric turbulent synthetic jets. *International Journal of Heat and Mass Transfer, 51*(25-26), 6194-6198. doi: https://doi.org/10.1016/j.ijheatmasstransfer.2008.04.011.

Alimohammadi, S., Fanning, E., Persoons, T., & Murray, D. B. (2016). Characterization of flow vectoring phenomenon in adjacent synthetic jets using CFD and PIV. *Computers and Fluids, 140*, 232-246. doi: 10.1016/j.compfuid.2016.09.022.

Amity, M., Honohan, T. M., & Glezer, A. (1997, June 29 – July 2). Modification of the aerodynamics characteristics of bluff bodies using fluidic actuators. In *Proceedings of 28th Fluid Dynamics Conference* (p. 2004). Snowmass Village, CO, USA. doi: https://doi.org/10.2514/6.1997-2004.

Batikh, A., Caen, R., Colin, S., Kourta, A., & Boisson, H. (2008). Numerical and Experimental study of micro synthetic jets for active flow control. *International Journal of Heat and Technology, 26*(1), 139-145. *doi: 10.18280/ijht.260119*.

Bayomy, A. M., & Saghir, M. Z. (2017). Experimental and Numerical study of the heat transfer characteristics of aluminum metal foam (with/without channels) subjected to steady water flow. *Pertanika Journal of Science and Technol*ogy, *25*(1), 221-246.

Cater, J. E., & Soria, J. (2002). The evaluation of round zero-net-mass-flux jets. *Journal of Fluid Mechanics, 472*,167-200. doi: 10.1017/S0022-1120 (02)00226-4.

Chandratilleke, T. T., Jagannatha, D., & Narayanaswamy, R. (2010). Heat transfer enhancement in micro channels with cross-flow synthetic jets. *International Journal of Thermal Sciences, 49*, 504-513. doi: https://doi.org/10.1016/j.ijthermalsci.2009.09.004.

Crook, A., Sadri, A. M., & Wood, M. J. (1999, June 28 – July 1). The development and implementation of synthetic jets for the separated flow. In *Proceedings of 17th Applied Aerodynamics Conference* (p. 3176). Norfolk, VA, USA. doi: https://doi.org/10.2514/6.1999-3176.

Dauphinee, T. M. (1957). Acoustic air pump. *Review of Science Instrument*, *28*(6), 452-452. doi: https://doi.org/10.1063/1.1715904.

Deepak, D., Jodel, A. Q., Cornelio, Midhun, A. M., & Prasad, S. U. (2017). Numerical analysis of the effect of nozzle geometry on flow parameters in abrasive water jet machines. *Pertanika Journal of Science and Technology, 25*(2), 497-506.

Giachetti, B., Fenot, M., Couton, D., & Plourde, F. (2018). Influence of Reynolds Number synthetic jet dynamics in cross flow configuration on heat transfer enhancement. *International Journal of Heat and Mass Transfer*, *118*, 1-13. doi: https://doi.org/10.1016/j.ijheatmasstransfer.2017.10.097.

Gillespie, M. B., Black, W. Z., Rinehart, C. A., & Glezer, A. (2006). Local convective heat transfer from a constant heat flux flat plate cooled by synthetic air jets, *Journal of Heat Transfer, 128*(10), 990-1000. doi: 10.1115/1.2345423.

Greco, C. S., Paolillo, G., Ianiro, A., Cardone, G., & De-Luca, L. (2018). Effects of the Stroke Length and nozzle- to-plate distance on synthetic jet impingement heat transfer. *International Journal of Heat and Mass Transfer, 117*, 1019-1031. doi: https://doi.org/10.1016/j.ijheatmasstransfer.2017.09.118.

Greco, C. S., Castrillo, G., Crispo, C. M., Astarita, T., & Cardone, G. (2016). Investigation of impinging single and twin circular synthetic jet flow field. *Experimental Thermal and Fluid Sciences, 74*, 364-367. doi: http://dx.doi.org/10.1016/j.expthermflusci.2015.12.019.

Holman, R., Utturkar, Y., Mittal, R., Smith, B. L., & Cattafesta, L. (2005). Formation criterion for synthetic jets. *American Institute of Aeronautics and Astronautics Journal, 43*(10), 2110-2115. doi: https://doi.org/10.2514/1.12033.

Holman, R., Gallas, Q., Carrol, B., & Cattafesta, L. (2003, June 23-26). Interaction of adjacent synthetic jets in airfoil control application. In *Proceedings of 33rd American Institute of Aeronautics and Astronautics* (p. 3709)*.* Orlanda, Florida, USA. doi: https://doi.org/10.2514/6.2003-3709.

Im, D. K., Choi, S., McClure, J., & Park, S. H. (2017). Numerical analysis of synthetic jet flows using a diagonally implicit harmonic balance method with preconditioning. *Journal of Computers and Fluids, 147*(2), 12-24. doi: https://doi.org/10.1016/j.compfluid.2017.01.022.

Jagannatha, D., Narayanaswamy, R., & Chandratilleke, T. T. (2009). Analysis of a synthetic jet- based electronic cooling module. *Numerical Heat Transfer, Part A, 56*(3), 211-229. doi: http://dx.doi.org/10.1080/10407780903163702.

Jain, M., Puranik, B., & Agrawal, A. (2011). A numerical investigation of effects of cavity and orifice parameters on the characteristics of synthetic jet flow. *Sensors and Actuators A physical, 165*(2), 351-366. doi: https://doi.org/10.1016/j.sna.2010.11.001.

Mclean, J. D., Crouch, J. D., Stoner, R. C., Sakurai, S., Seidel, G. E., Feifel, W. M., & Rush, H. M. (1999). *Study of the application of separation control by unsteady excitation to civil transport aircraft* (Report No. NASA/CR-1999-209338). Hampton, Virginia: National Aeronautics and Space Administration.

Paolillo, G., Greco, C. S., & Cardone, G. (2017). The evolution of quadruple synthetic jets. *Journal of Experimental Thermal and Fluid Science, 89*, 259-275. doi: https://doi.org/10.1016/j.expthermflusci.2017.08.010.

Qayoum, A., Gupta, V., Panigrahi, P. K., & Muralidhar, K. (2010a). Perturbation of laminar boundary layer by synthetic jet for heat transfer enhancement. *International Journal of Heat and Mass Transfer, 53*(23-24), 5035-5057. doi: https://doi.org/10.1016/j.ijheatmasstransfer.2010.07.061

Qayoum, A., Gupta, V., Panigrahi, P. K., & Muralidhar, K. (2010b). Influence of amplitude and frequency modulation on flow created by a synthetic jet actuator. *Sensors and Actuators A Physical, 162*(1), 36-50. doi: https://doi.org/10.1016/j.sna.2010.05.008.

Rathnasingham, R., & Breuer, K. S. (2003). Active control of turbulent boundary layers. *Journal of Fluid Mechanics, 495*, 209-233. doi: https://doi.org/10.1017/S0022112003006177.

Silva-Llanca, L., Ortega, A., & Rose, I. (2015). Experimental convective heat transfer in a geometrically large two-dimensional impinging synthetic jet. *International Journal of Heat and Mass Transfer, 90*, 339-350. https://doi.org/10.1016/j.ijthermalsci.2014.11.011.

Smith, B., & Glezer, A. (1998). The formation and evolution of synthetic jets. *Physics of Fluids*, 10(9), 2281-2297. doi: https://doi.org/10.1063/1.869828.

Utturkar, Y., Holman, R., Mittal, R., Carroll, B., Sheplak, L., & Cattafesta, M. (2003, January 6-9). A jet formation criterion for synthetic jet actuators. In *Proceedings 41st Aerospace Sciences Meeting and Exhibit* (p. 636). Reno, Nevada. doi: https://doi.org/10.2514/6.2003-636.

Yuan-Wei, L., Jing-Zhou, Z., Yong, S., & Xiao-Ming, T. (2014). Numerical investigation for effects of actuator parameters and excitation frequencies on synthetic jet fluidic characteristics. *Sensors and Actuators A Physical, 219*, 100-111. doi: https://doi.org/10.1016/j.sna.2014.08.009.

Zhang, J. Z., & Tan, X. M. (2012). Experimental study on flow and heat transfer characteristics of synthetic jet driven by piezoelectric actuator. *Science in China Series E: Technogical Science, 50*(2), 221-229. doi: 10.1007/s11431-005-0006-1.

Zhou, J., & Zhong, S. (2009). Numerical simulation of the interaction of a circular synthetic jet with a boundary layer. *Journal of Computer and Fluids, 38*(2), 393-405. doi: https://doi.org/10.1016/j.compfluid.2008.04.012